Res Chem Intermed (2015) 41:9845–9862
DOI 10.1007/s11164-015-1988-3

Novel crosslinked and zeolite-filled polyvinyl alcohol membrane adsorbents for dye removal

Raziyeh Ghahremani[1] · Bahareh Baheri[1] · Mohammad Peydayesh[1] · Shirin Asarehpour[1] · Toraj Mohammadi[1]

Received: 20 November 2014 / Accepted: 22 February 2015 / Published online: 4 April 2015

Abstract In order to enhance adsorption capacity for dye removal, mixed matrix SAPO-34/polyvinyl alcohol membrane adsorbent (MMMA) was synthesized. Mixing PVA with SAPO-34 particles provides an effective structure that leads to efficient adsorption performance and high methylene blue removal efficiency. The effect of zeolite content was also studied via synthesis of different MMMAs. Morphology and intermolecular interaction of the MMMAs were determined using fourier transform infrared and scanning electron microscope. The adsorption measurements were carried out in batch mode at various operating parameters such as contact time, temperature, pH, and initial concentration to determine the optimum experimental condition. The experimental data were closely fitted with the Freundlich adsorption isotherm model rather than the Langmuir and the Temkin isotherm models and the adsorption kinetic data were fitted in accordance with the pseudo-second-order model. The evaluated data for ΔG° indicated that the adsorption process is spontaneous at lower temperature values and non-spontaneous at higher temperature values. Estimated ΔH° and ΔS° values also exhibited an exothermic adsorption process with an increase in orderliness at the solid–solution interface.

Keywords Membrane adsorbent · Dye removal · SAPO-34-zeolite particles · PVA

Introduction

Among countless industrial contaminations that are released in developed countries, dyes and their derivatives are the more obvious water pollutants that have many negative consequences on the environment and living organisms. Discharging

✉ Toraj Mohammadi
torajmohammadi@iust.ac.ir

[1] Research and Technology Centre for Membrane Processes, Faculty of Chemical Engineering, Iran University of Science and Technology (IUST), Narmak, Tehran, Iran

colored wastes into effluents not only disturbs nature aesthetically, but it also prevents sunlight penetration and interrupts ecosystem and photosynthesis processes [1]. Dye removal processes can be performed with physical, chemical, and biological methods such as filtration, flocculation, electrochemical oxidation, ozonation, and biosorption [2]. Traditional biological and chemical methods are sometimes not pragmatic because of non-biodegradability of synthetic dyes. The adsorption process is the most effective, economical, and flexible method, as it does not generate any other harmful materials [3]. In the adsorption process, the adsorbent is applied as a material that is able to bind the toxic substances to its surface [4]. The surface of an adsorbent can be functionalized for enhancing its performance and adsorbent tendency toward toxic substances [5]. Although powder of activated carbon and different biomaterials has been used as a proper adsorbent for several years, using fine powder produces a large amount of sludge, which may cause harmful effects on the environment [3]. Therefore, developing some processes that are environmentally friendly and economical is essential in the wastewater treatment industry. Membrane adsorption has been established as a suitable choice for this purpose. This is a new and developed field including both membrane technology and adsorption process. This method also has some unique advantages like resistance toward temperature, hostile microbial assail, and harmful chemical component. Another advantage of this method is that membrane adsorbent affinity toward some toxic target components can be improved by changing the membrane characteristics [6]. Mixed matrix membranes (MMMs) are composite polymeric membranes incorporated with inorganic materials such as zeolites as fillers, which benefit from both of polymeric and inorganic structures. Using zeolite particles solely or in the form of membrane is expensive, and suffers from long preparation time and complex methods [7]. However, the enlarged surface area of zeolites makes them the best choice to improve adsorption performance and capacity of the MMMAs [8]. In the current study for the sake of applying an economical adsorption process that reduces environmental problems and improves dye removal efficiency, PVA was mixed with different amounts of SAPO-34-zeolite particles to form MMMAs with the higher removal performance in comparison to the neat PVA membrane.

Experimental

Materials

PVA (98 %, molecular weight = 145,000), glutaraldehyde (GA, 50 wt%), methylene blue (MB), phosphoric acid (H_3PO_4, 85 wt% aqueous solution), aluminum triisopropylate (Al(i-C_3H_7O)3, >98 %), and tetra-ethyl ammonium hydroxide (TEAOH, 20 wt% aqueous solution) were purchased from Merck (Darmstadt, Germany). Ludox AS-40 colloidal silica sol (SiO_2, 40 wt% aqueous solution) was purchased from Sigma Aldrich. Distilled water was used in all the experiments. SAPO-34 zeolite was synthesized using double-distilled water.

Preparation of SAPO-34-zeolite particles

SAPO-34 seed crystals were synthesized hydrothermally from a gel with a molar composition of $1.0Al_2O_3$:$1.0P_2O_5$:$0.6SiO_2$:1.2TEAOH:$55H_2O$ as described by Li et al. [9]. The solution of H_3PO_4 and H_2O was stirred for 2–3 min in a 50-ml Pyrex beaker and then Al(i-$C_3H_7O)_3$ was added slowly to the resulted solution while the beaker was located in an ice bath. The beaker was sealed and stirred for 10–12 h. After adding the organic template, TEAOH, to the solution and stirring for 45 min, the colloidal silica also was added to the mixture. In order to obtain a homogenous gel, the beaker was sealed and the solution was stirred for 48 h at room temperature. The pH of the above synthesis solution was measured as 7 before being transferred to a Teflon-lined stainless-steel autoclave. The hydrothermal treatment was carried out at 180 °C for 24 h. When crystallization was finished, the solution was cooled to room temperature and it was centrifuged with distilled water in order to separate the seeds at 3500 rpm for 15 min. This procedure was executed two times. The resulting precipitate was dried overnight at 100 °C under vacuum condition. In this experiment, due to the presence of water in the separating mixture and preventing blockage of SAPO-34 pores by water molecules, the samples were not calcined [10–12].

Membrane preparation

A proper amount of the double-distilled water was heated to 95 °C. The PVA powder was then sprinkled to the hot water slowly, while it was magnetically stirred strongly. The beaker was covered with plastic wrap and stirred until the solution was cleared. Then, the solution was cooled down to ambient temperature and a certain amount of GA as crosslinker (0.05 mol for each mole of PVA monomeric unit) was added to the solution. After that, the uncalcined SAPO-34-zeolite particles with 0, 5, 10, 15, and 20 wt% of the polymer were dispersed in the double-distilled water, and sonicated for 1 h (Hilsonic, Birkenhead, United Kingdom). The SAPO-34 solution was then added to the polymer solution and gently stirred at room temperature for 2 h. Afterwards, the 10 wt% polymer solution was casted over a glass plate with the aid of a casting knife. The membranes were placed in a dust-free environment at room temperature for 24 h to evaporate the solvent. The dried membranes were heated in an oven and held at about 150 °C for 1 h to complete the crosslinking reactions [13, 14]. The zeolite-filled membranes were also compared with the neat PVA membrane (0 wt% SAPO-34).

All the membranes were as thick as of 50 μm (Mitutoyo Model MDC-25SB digital micrometer, 1-μm accuracy). They were cut into a 0.5 × 0.5-cm^2 squarish shape to be utilized in the adsorption experiments.

Adsorption experiments

In order to carry out the adsorption experiments, the batch procedure was used. A stock solution of MB at concentration of 500 mg L^{-1} was prepared by dissolving precisely weighted MB in the double-distilled water. This was then diluted to prepare other different concentrations. All the experiments were performed using

the adsorbent dosage of 1 g L^{-1} and the solutions' pH levels were adjusted to desired values by adding dropwise a small amount of diluted NaOH or HCl. The solutions were stirred with a magnetic stirrer at 350 rpm and 25 °C. To determine the dye removal efficiency of the membrane adsorbent, concentration of solutions was specified using a double beam UV–visible spectrophotometer Shimadzu UV-1800 at characteristic wavelength of 633 nm. The amount of dye adsorbed per unit mass of the adsorbent (q_e) and the percentage dye removal efficiency ($R\%$) were calculated using the following equations, respectively:

$$q_e = \frac{(C_0 - C_e)V}{M} \quad (1)$$

$$R\% = \frac{(C_0 - C_e)}{C_0} \times 100 \quad (2)$$

where C_0 and C_e (mg L^{-1}) are initial and final concentrations of dye, V (L) is volume of the dye solution and M (g) is weight of the membrane adsorbent which were used in this research.

Results and discussion

Morphology and structural characterization of SAPO-34 particles and MMMAs

A scanning electron microscope (SEM) image of the SAPO-34 particles is shown in Fig. 1. As observed, the particles have an average size of 1–2 μm and have smooth external surfaces with a cubic shape morphology, which is typical for the SAPO-34

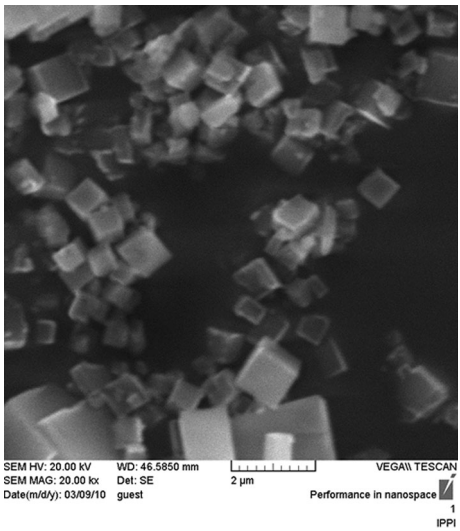

Fig. 1 SEM image of the SAPO-34-zeolite particles

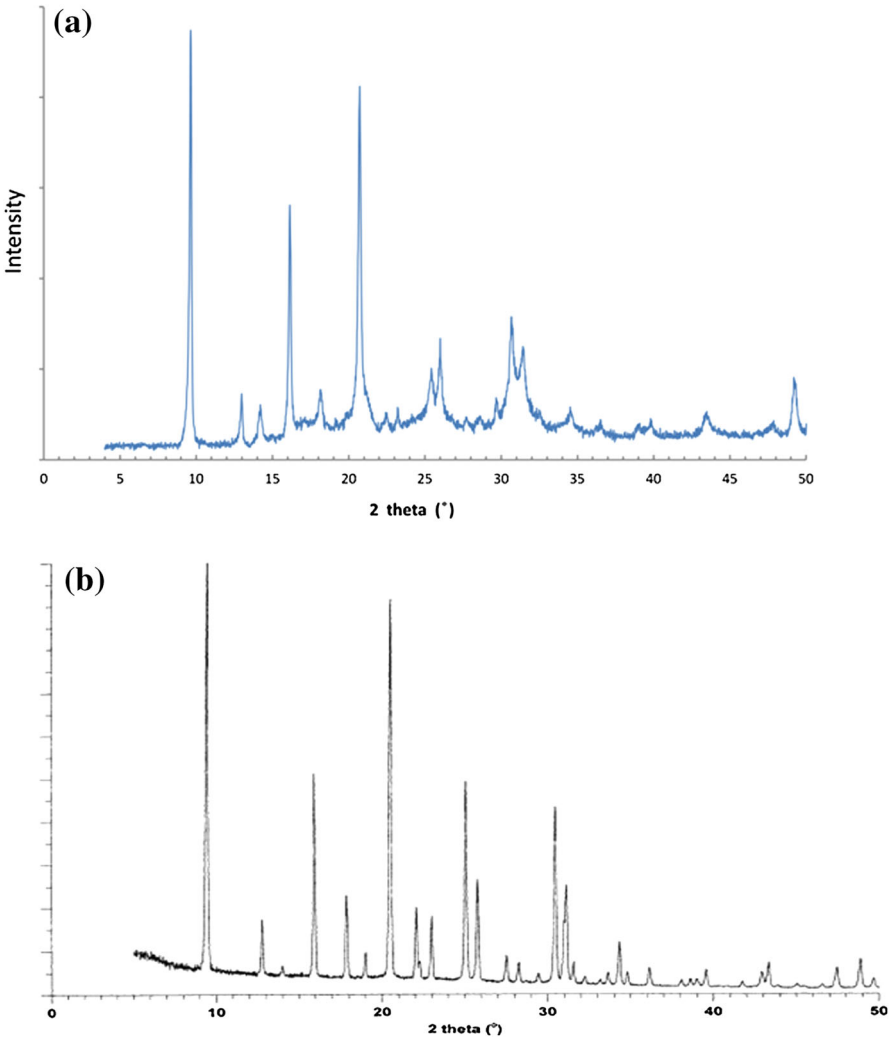

Fig. 2 XRD pattern of the SAPO-34-zeolite particles (**a**) and the standard XRD pattern of SAPO-34 molecular sieve (**b**)

crystals. XRD pattern of the SAPO-34 particles is presented in Fig. 2a. The XRD pattern represents the characteristic peaks of the SAPO-34 phase ($2\theta = 9.52, 20.55$, and double peaks at $2\theta = 25$ and $2\theta = 31$) confirming its formation. The standard XRD pattern of SAPO-34 molecular sieve is also presented in Fig. 2b [15].

Figure 3 shows cross-sectional and surface SEM images of the MMMAs at 10 wt% zeolite loading at high magnification. The membrane morphology was examined with a CamScan SEM (Model MV2300) microscope. The images clearly demonstrate that the SAPO-34 particles are dispersed excellently through the polymer structure and the membrane surface is defect free. Regarding the SEM

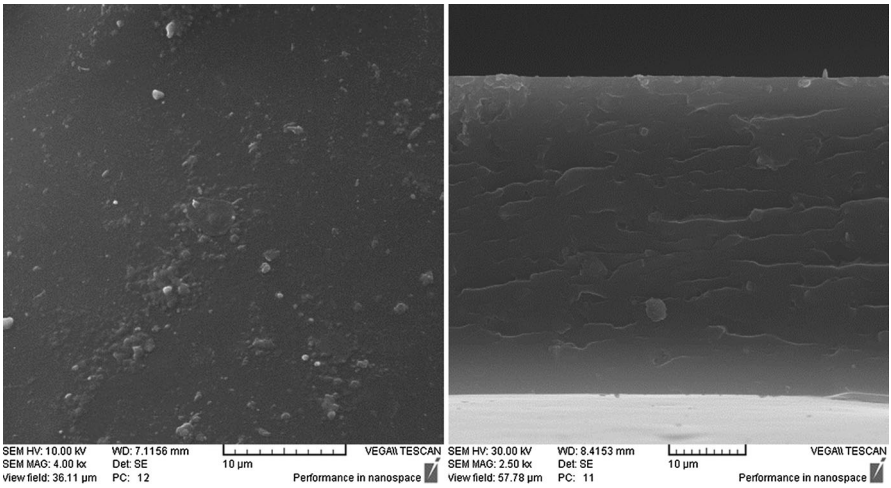

Fig. 3 Cross-sectional and surface SEM images of the MMMAs at 10 wt% zeolite loading

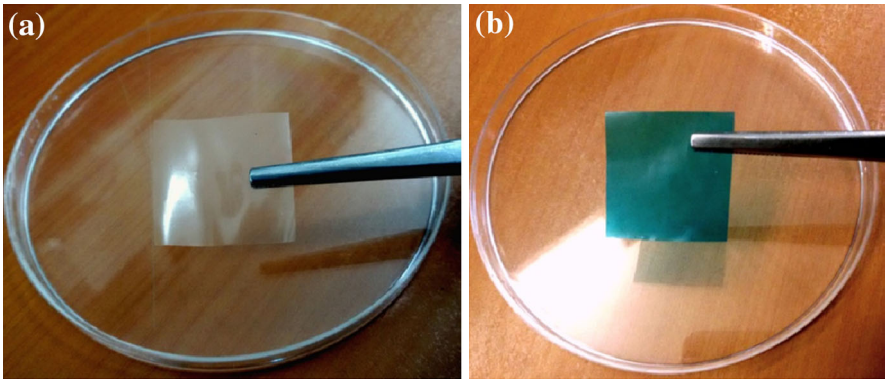

Fig. 4 Digital image of MMMAs before (**a**) and after (**b**) adsorption experiment

images, there is a good adhesion between the SAPO-34 particles and the polymer matrix. Figure 4 depicts a digital image of MMMAs before and after adsorption experiment.

Fourier transform infrared (FTIR) spectra of the MMMAs are displayed in Fig. 5, after and before MB adsorption. The extensive absorption peak, which is exhibited at 3310 cm^{-1}, correlates to the O–H stretching vibration of the hydroxyl group of PVA and zeolite. The Si–O stretching is revealed by the sharp intense band at around 1098 cm^{-1}. Several bands between 500 and 1000 cm^{-1} are due to the presence of SAPO-34, which causes the stretching of Al–O vibrations. The peak that is detected at 2924 cm^{-1} is assigned to the stretching vibration of C–H bond. These characteristic changes, which are disclosed in the FTIR spectrum of MMMAs

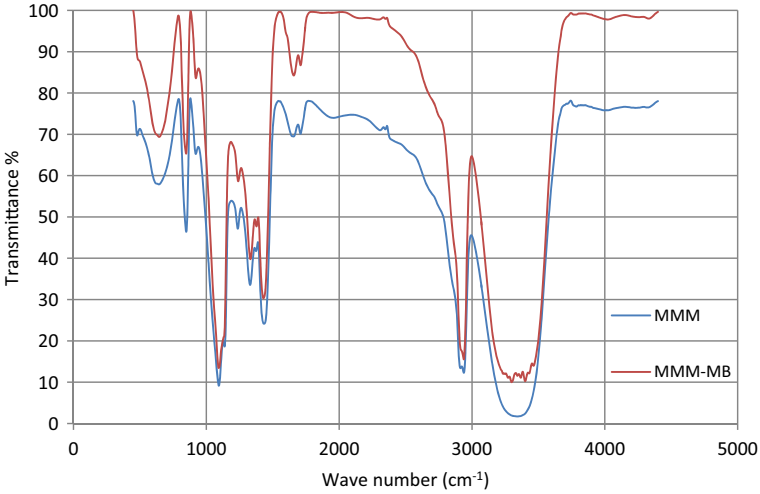

Fig. 5 FTIR spectra of the MMMAs before and after MB adsorption

after MB adsorption, imply that some peaks are transferred or disappear, and new peaks are also found. These changes verify the MB interactions with the functional groups of the MMMAs in the adsorption process [16].

Effect of SAPO-34-zeolite loading on MB adsorption

The strong electrostatic forces between SAPO-34 zeolite particles and MB molecules make SAPO-34 one of the best candidates as filler in MMMAs. The adsorption data for MB onto the SAPO-34 powder is presented in Table 1. The experiment was performed at a temperature of 25 °C, pH of 6, and MB concentration of 10 mg L^{-1}.

To enhance MB adsorption on PVA membrane, the experiments were performed by mixing different ratios of SAPO-34 particles to the PVA to form MMMAs. As observed in Fig. 6, increasing the SAPO-34 particles content from 5 to 20 wt% increases the q_e values from 5.50 to 8.23 mg g^{-1} and the removal efficiency from 48.07 to 71.86 % at a temperature of 25 °C, pH of 6, and MB concentration of 10 mg L^{-1}. It is clear that adding the porous zeolite particles to the dense polymer matrix enhances the MMMAs adsorption surface, leading to higher dye removal efficiency. Besides, the major adsorption mechanism in this process is electrostatic

Table 1 Adsorption data of SAPO-34 powder at pH of 6, initial MB concentration of 10 mg L^{-1}, temperature of 25 °C, and contact time of 180 min

SAPO-34 powder	
Q (mgg^{-1})	Removal (%)
4.88	90

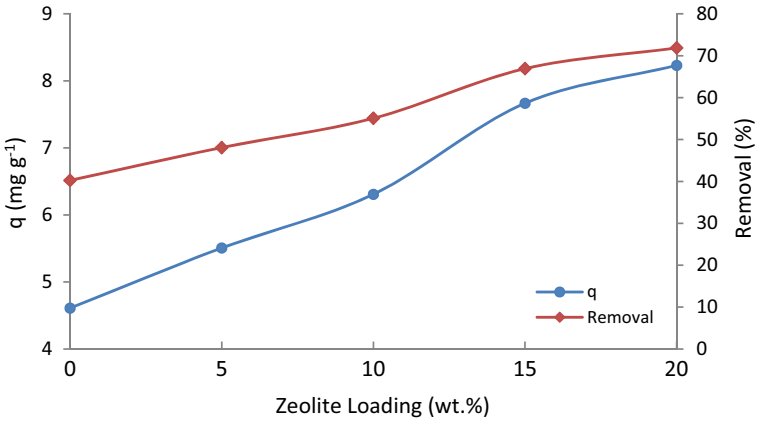

Fig. 6 Effect of zeolite loading on MB adsorption at pH of 6, initial MB concentration of 10 mg L^{-1}, temperature of 25 °C, and contact time of 180 min

interaction between SAPO-34 particles and cationic dye. Hence, increasing the SAPO-34 particles content in MMMAs enhances their adsorption capacity and performance.

Effect of contact time on MB adsorption

As observed in Fig. 7, the adsorption process meets the equilibrium after 180 min. This manner of acting can be illustrated as a two-step kinetic behavior, a fast initial adsorption followed by a slow adsorption. Accelerating behavior of dye adsorption at first 15 min is due to the huge affinity between MB molecules and the MMMAs.

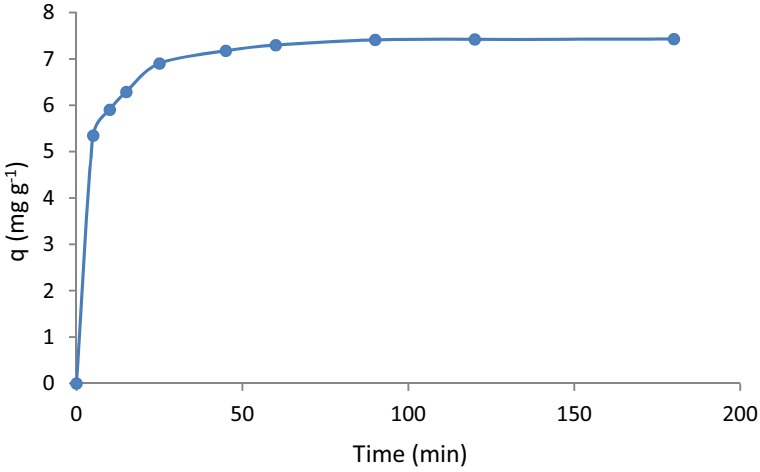

Fig. 7 Effect of contact time on MB adsorption at pH of 6, initial MB concentration of 10 mg L^{-1}, and temperature of 25 °C

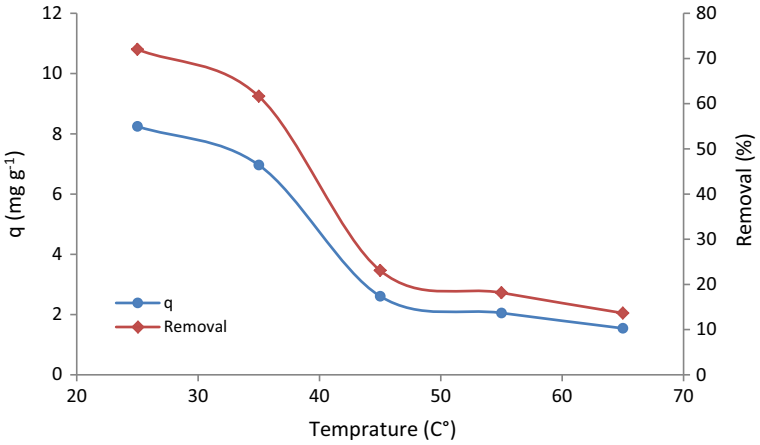

Fig. 8 Effect of temperature on MB adsorption at pH of 6, initial MB concentration of 10 mg L^{-1} and contact time of 180 min

It is worth stating that at the start of the adsorption process, all adsorbent sites are unfilled, leading to a high solute concentration gradient. By reducing the vacant sites of the adsorbent and forming the probable monolayer of MB molecules on the MMMAs surface, the adsorption process proceeds slowly toward the equilibrium.

Effect of temperature on MB adsorption

In order to demonstrate the influence of temperature, adsorption experiments were performed at 25, 35, 45, 55, and 65 °C, respectively. As observed in Fig. 8, increasing the temperature from 25 to 65 °C decreases the adsorption capacity from 8.24 to 1.54 mg g^{-1} and the removal efficiency from 72.01 to 13.65 %, respectively, at pH of 6, MB concentration of 10 mg L^{-1} and 20 wt% zeolite loading. The highest adsorption capacity was obtained at 25 °C, confirming less interaction between MB molecules and active chemical groups of the MMMA at higher temperature, and demonstrating the adsorption process of MB molecules onto the MMMA is exothermic.

Effect of pH solution on MB adsorption

The effect of pH on the MB adsorption by MMMAs is shown in Fig. 9. The adsorption mechanism is electrostatic forces between MB and SAPO-34 particles' surface. As reported by Heyden et al., SAPO-34 particles in water at pH of 4 and higher have negative zeta potential [17]. Therefore, the electrostatic attraction between cationic dyes and the zeolite surface greatly increases the adsorption capacity [18]. Changing pH not only influences the surface charge of the MMMAs, but also the degree of ionization of MB molecules in the solution. At the higher pH values, the negatively charged groups on the surface of MMMAs are enhanced leading to the higher inclination of MB positive charged ions to bind with the MMMAs. Adversely, the positively charged groups of MMMAs hinder the

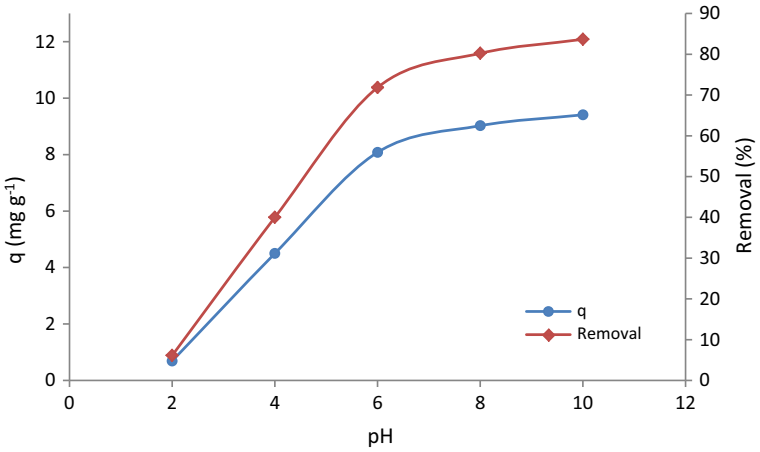

Fig. 9 Effect of pH on MB adsorption at the initial MB concentration of 10 mg L^{-1}, the temperature of 25 °C, and the contact time of 180 min

adsorption of the cationic dyes like MB in acidic mediums at the lower pH values. As a result, at the higher pH mediums, the competition between protons (H^+) and MB molecules toward the adsorbent is diminished. In these experiments, by increasing the pH value from 2 to 10, the MB adsorption and the removal efficiency enhance from 0.68 to 9.41 mg g^{-1} and 6.11 to 83.66 %, respectively at temperature of 25 °C, MB concentration of 10 mg L^{-1} and 20 wt% zeolite loading [3, 19].

Effect of initial MB concentration on MB adsorption

The influence of initial MB concentration on the MB adsorption is presented in Fig. 10. It is clear that by increasing the initial MB concentration, the adsorption capacity enhances. As observed, when the initial MB concentration increases from 5 to 100 mg L^{-1}, the

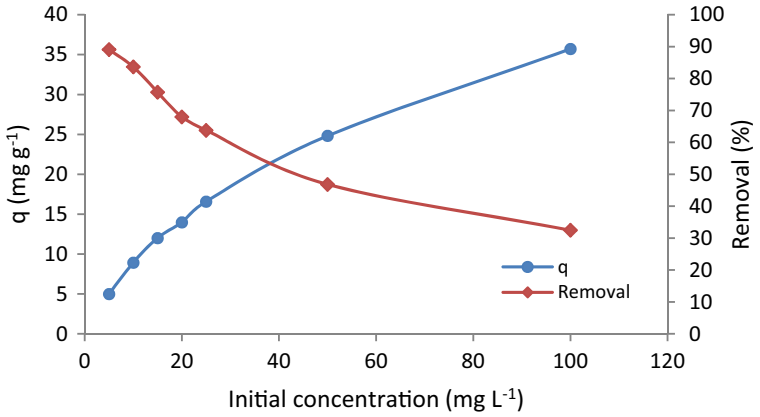

Fig. 10 Effect of initial concentration on MB adsorption at pH of 10, temperature of 25 °C, and contact time of 180 min

amount of MB adsorbed at equilibrium increases from 4.99 to 35.71.84 mg g^{-1}, while the removal efficiency decreases from 89.09 to 32.47 % at temperature of 25 °C, pH of 10, and 20 wt% zeolite loading. Increasing the initial MB concentration leads to greater mass transfer driving force and higher MB adsorption, while reducing the available adsorption sites declining the dye removal efficiency [3, 20].

Adsorption kinetics

In order to determine the adsorption kinetic mechanism of MB to the MMMAs, the pseudo-first-order, pseudo-second-order, and the intraparticle diffusion models were used to fit the experimental data.

The following equation illustrates the pseudo-first-order kinetic model [21]:

$$\log(q_e - q_t) = \log q_e - \frac{k_{pf}}{2.303} t \tag{3}$$

where k_1 (min^{-1}) is the rate constant of pseudo-first order and q_t (mg g^{-1}) and q_e (mg g^{-1}) are the amounts of dye adsorbed at time t (min) and equilibrium, respectively. As depicted in Fig. 11a, the values of k_1 and q_e were determined from the slope and the intercept of this plot.

The pseudo-second-order kinetic model is described with the following equation [21]:

$$\frac{t}{q_t} = \frac{1}{k_{ps} q_e^2} + \frac{t}{q_e} \tag{4}$$

where k_{ps} (g mg^{-1} min^{-1}) is the rate constant of pseudo-second order. As presented in Fig. 11b, the values of k_{ps} and q_e were estimated from the intercept and slope of this plot.

The following equation was used to evaluate the initial rate of adsorption, h (mg g^{-1} min^{-1}), for the pseudo-second-order model [22]:

$$h = k_{ps} q_e^2 \tag{5}$$

The intraparticle diffusion model can be expressed using the following equation [23]:

$$q_t = k_p t^{1/2} + C \tag{6}$$

where C is the intercept and k_p is the intraparticle diffusion rate constant (mg g^{-1} $min^{-1/2}$). They were determined from the intercept and the slope of the plot (Fig. 11c). The kinetic data were fitted by the kinetic equation models as referred above and tabulated in Table 2.

The value of correlation coefficient (R^2) obtained from the pseudo-second-order kinetic (0.9999) was more than those obtained from the pseudo-first-order kinetics (0.9862) and the intraparticle diffusion model (0.8203). The values of $q_{e.2.cal}$ were found to agree well with the experimentally provided data ($q_{e.exp}$). Therefore, the pseudo-second-order kinetic plausibly demonstrates the dye adsorption on MMMAs. The pseudo-second-order model is based on the assumption that the rate-limiting step may be chemical sorption or chemisorption involving valence forces through sharing or exchanging of electrons between sorbent and sorbate [24].

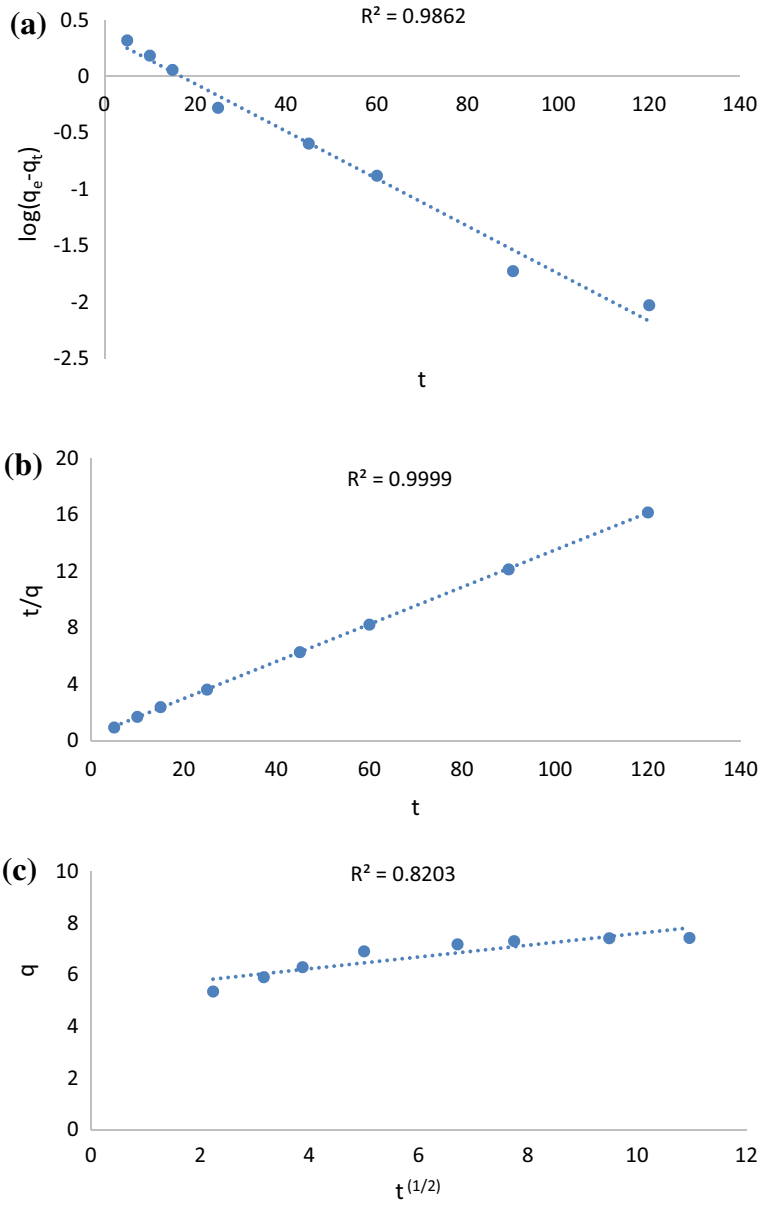

Fig. 11 Adsorption kinetics of MB adsorbed by MMMAs: **a** pseudo-first-order model, **b** pseudo-second-order model, and **c** intraparticle diffusion model

Adsorption isotherms

Three models were applied to determine the adsorption parameters: Langmuir, Freundlich, and Temkin isotherm models. The Langmuir isotherm model, which

Table 2 Adsorption kinetics parameters for MB onto the MMMAs

Experiment	Pseudo-first-order			Pseudo-second-order			Intraparticle model		
$q_{e,exp}$ (mg g^{-1})	K_{pf} (min^{-1})	$q_{e.1.cal}$ (mg g^{-1})	R^2	K_{ps} (g mg^{-1} min^{-1})	$q_{e.2.cal}$ (mg g^{-1})	R^2	k_{id} (mg g^{-1} $min^{-1/2}$)	C (mg g^{-1})	R^2
7.4302	0.0483	2.261	0.9862	0.0503	7.5987	0.9999	0.2276	5.3193	0.8203

presumes the monolayer sorption onto a surface with a limited number of uniform sites, can be expressed using the following equation [25]:

$$\frac{C_e}{q_e} = \frac{C_e}{q_{max}} + \frac{1}{K_L q_{max}} \tag{7}$$

where q_e is the dye concentration onto the adsorbent (mg g^{-1}) at equilibrium and q_{max} is the maximum adsorption capacity (mg g^{-1}). C_e is the dye concentration at equilibrium in the solution (mg L^{-1}). K_L is the Langmuir constant (L mg^{-1}) related to the affinity of binding sites and the free energy of adsorption. The slope and intercept of the delineated straight line (C_e/q_e versus C_e) specify the values of q_{max} and K_L, respectively (Fig. 12a).

The Langmuir isotherm can be demonstrated by a constant dimensionless factor named as the equilibrium parameter (R_L):

$$R_L = \frac{1}{1 + K_L C_0} \tag{8}$$

If $0 < R_L < 1$, it indicates favorable adsorption while $R_L > 1$, $R_L = 1$ and $R_L = 0$ implies unfavorable adsorption; linear adsorption and irreversible adsorption processes, respectively [22].

The relationship between R_L and initial MB concentration is demonstrated in Fig. 12b. The estimated values of R_L for all initial concentrations of MB are <1 and >0, implying a favorable adsorption process.

The experimental Freundlich equation for adsorption on a heterogeneous surface is generally described using the following formula [26]:

$$\ln q_e = \ln K_F + \frac{1}{n} \ln C_e \tag{9}$$

K_F and n are the Freundlich constants evaluated by plotted ln q_e versus ln C_e. K_F $((mg/g)/(mg/L)^{1/n})$ indicates sorption capacity and n refers to the sorption intensity of the system (Fig. 12c).

By fitting the experimental data with the Temkin isotherm model, the enthalpy of the adsorption and the adsorbent–adsorbate interactions were revealed. The Temkin isotherm equation in linear form can be presented as follows [22]:

$$q_e = \frac{RT}{b_T} \ln K_T + \frac{RT}{b_T} \ln C_e \tag{10}$$

where T is absolute temperature (K), R is gas universal constant [8.314 J/(mol K)], b_T (J/mol) is the Temkin constant related to enthalpy of adsorption and K_T (L g^{-1}) is the equilibrium binding constant. The Temkin constants b_T and K_T were determined using the slope and intercept of the plotted q_e versus ln C_e (Fig. 12d).

Using these isotherm equations, the adsorption equilibrium data were estimated and correlating evaluated parameters were organized in Table 3.

The value of R^2 obtained from the Freundlich isotherm Eq. (0.9927) was higher than those obtained from the Langmuir (0.9754) and the Temkin (0.9377) isotherm equations. It is very clear that the Freundlich isotherm model, which represents an adsorption process on a heterogeneous surface and a multilayer adsorption with

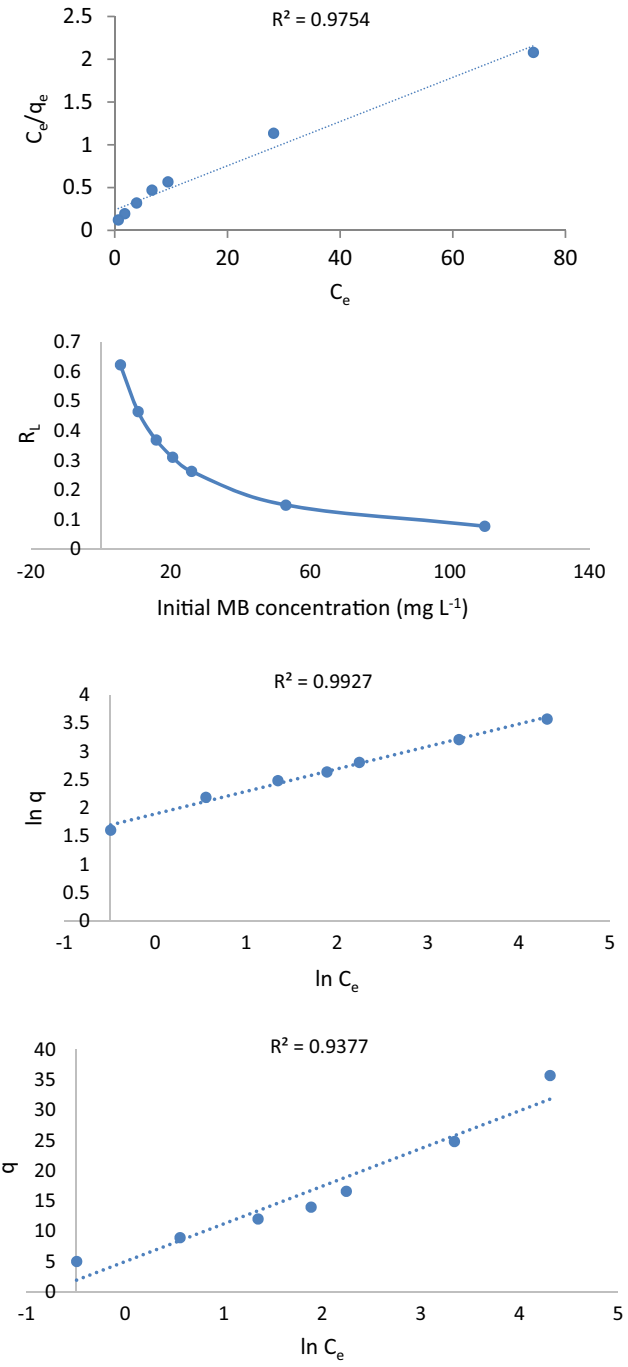

Fig. 12 Langmuir isotherm (**a**) and relationship between initial MB concentration and R_L (**b**), Freundlich (**c**), and Temkin (**d**) isotherms of MB adsorption onto the MMMAs

Table 3 Adsorption isotherm parameters for MB onto the MMMAs

Langmuir			Freundlich			Temkin		
q_m (mg g^{-1})	K_L (L mg^{-1})	R^2	K_F (mg/g)(L/mg)$^{1/n}$	n	R^2	b_T (J mol^{-1})	K_T (L g^{-1})	R^2
38.7597	0.1078	0.9754	6.6612	2.5144	0.9927	444.821	2.2291	0.9377

interactions between adsorbed molecules, can properly verify the MB adsorption on the MMMAs. The adsorption forces for the multi-layer adsorption of MB on MMMAs are divided into two types, MB–MB and MB-MMMA interactions. The first layer adsorption is influenced by the interaction between MB and MMMA. However, the adsorption of the other layers is due to the majority of MB–MB interactions and the minority of MB–MMMAs interactions [27].

Adsorption thermodynamics

Thermodynamics parameters like difference in standard free energy (ΔG°), enthalpy (ΔH°), and entropy (ΔS°) were determined using the following formulas for the MB adsorption process [28]:

$$K_D = \frac{q_e}{C_e} \tag{11}$$

$$\Delta G^{\circ} = -RT \ln K_D \tag{12}$$

$$\ln K_D = \frac{\Delta S^{\circ}}{R} - \frac{\Delta H^{\circ}}{RT} \tag{13}$$

The values of ΔH° and ΔS° were estimated from the slope and intercept of the delineated straight line of ln K_D versus 1/T (Fig. 13). Standard Gibbs free energy change of adsorption (ΔG°) can be evaluated using Eq. (12).

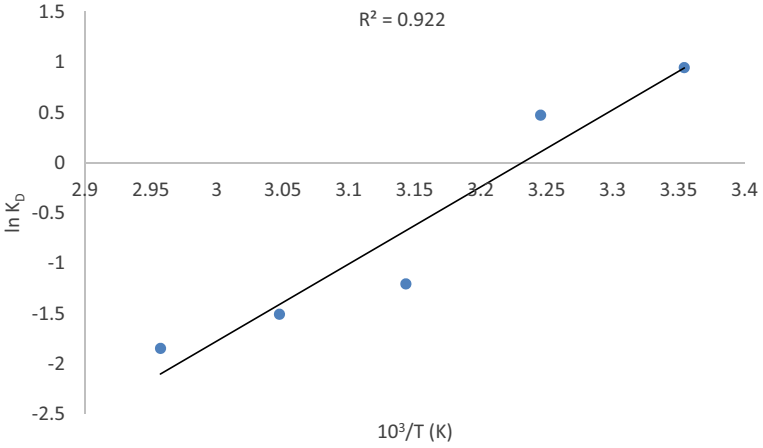

Fig. 13 Van't Hoff plot for the adsorption of MB onto the MMMAs

Table 4 Adsorption thermodynamics parameters for MB onto the MMMAs

$\Delta H°$ (kJ mol^{-1})	$\Delta S°$ (J mol^{-1} K^{-1})	$\Delta G°$ (kJ mol^{-1})				
		298	308	318	328	338
−63.7318	−205.929	−2.3339	−0.2746	1.7846	3.8439	5.9032

The calculated thermodynamics parameters are arranged in Table 4. The negative Gibbs free energy change ($\Delta G°$) at lower temperature implies a spontaneous adsorption process, while the positive evaluated data at higher temperature reveals that the adsorption process is non-spontaneous. The negative value of $\Delta H°$ also exhibits an exothermic adsorption process. In addition, the negative value of entropy change ($\Delta S°$) indicates a reduction in randomness and an enhancement in orderliness at the solid–solution interface during the adsorption process [21, 29].

Conclusions

In this work, the SAPO-34/polyvinyl alcohol mixed matrix membrane adsorbents (MMMAs) were prepared by mixing the various contents of SAPO-34 particles with PVA. By adding the zeolite particles, an effective structure of the membrane adsorbent was obtained representing an efficient and applicable adsorption capacity. By increasing the zeolite loading from 5 to 20 wt%, the MMMAs performance improves. In order to obtain the optimum condition, the experiments with the adsorbent dosage of 1 g L^{-1}were carried out in batch adsorption technique with various experimental parameters. The maximum q_e of 35.71 mg g^{-1} was achieved in temperature of 25 °C, pH of 10, initial MB concentration of 100 mg L^{-1} and 20 wt% zeolite loading and the highest removal efficiency of 89.10 % was attained at temperature of 25 °C, pH of 10, initial MB concentration of 5 mg L^{-1} and 20 wt% zeolite loading. As observed, increasing initial MB concentration from 5 to 100 mg L^{-1} and pH from 2 to 10 increases the adsorption capacity, while it declines at high temperature. Equilibrium data were fitted properly with the Freundlich isotherm equation and the rate of MB adsorption on the MMMAs was found to fit well with the pseudo-second-order model. Thermodynamics parameters exhibited that the adsorption process is exothermic and spontaneous at lower temperature and non-spontaneous at higher temperature. The novel MMMAs that were applied as a flexible and simple adsorbent for dye elimination encourage an efficient and environmentally friendly adsorption process.

References

1. S. Haider, F.F. Binagag, A. Haider, A. Mahmood, N. Shah, W.A. Al-Masry, S.U.-D. Khan, S.M. Ramay, Desalin. Water Treat. (2014). doi:10.1080/19443994.2014.926840

2. P. Kazemi, M. Peydayesh, A. Bandegi, T. Mohammadi, O. Bakhtiari, Chem. Pap. **67**, 722–729 (2013)
3. A. Aluigi, F. Rombaldoni, C. Tonetti, L. Jannoke, J. Hazard. Mater. **268**, 156–165 (2014)
4. S. Abadian, A. Rahbar-Kelishami, R. Norouzbeigi, M. Peydayesh, Res. Chem. Intermed. (2014). doi:10.1007/s11164-014-1851-y
5. R. Ansari, B. Seyghali, A. Mohammad-khah, M.A. Zanjanchi, Sep. Sci. Technol. **47**, 1802–1812 (2012)
6. T. Robinson, G. McMullan, R. Marchant, P. Nigam, Bioresour. Technol. **77**, 247–255 (2001)
7. M.U.M. Junaidi, C.P. Leo, A.L. Ahmad, S.N.M. Kamal, T.L. Chew, Fuel Process. Technol. **118**, 125–132 (2014)
8. M. Peydayesh, S. Asarehpour, T. Mohammadi, O. Bakhtiari, Chem. Eng. Res. Des. **91**, 1335–1342 (2013)
9. S. Li, J.L. Falconer, R.D. Noble, J. Membr. Sci. **241**, 121–135 (2004)
10. J.C. Poshusta, R.D. Noble, J.L. Falconer, J. Membr. Sci. **186**, 25–40 (2001)
11. J.C. Poshusta, R.D. Noble, J.L. Falconer, J. Membr. Sci. **160**, 115–125 (1999)
12. Y. Hirota, K. Watanabe, Y. Uchida, Y. Egashira, K. Yoshida, Y. Sasaki, N. Nishiyama, J. Membr. Sci. **415–416**, 176–180 (2012)
13. B. Baheri, M. Shahverdi, M. Rezakazemi, E. Motaee, T. Mohammadi, Chem. Eng. Commun. **202**, 316–321 (2014)
14. M. Shahverdi, B. Baheri, M. Rezakazemi, E. Motaee, T. Mohammadi, Polym. Eng. Sci. **53**, 1487–1493 (2013)
15. H. Robson, *Verified Synthesis of Zeolitic Materials*, 2nd edn. (Elsevier Science, Amsterdam, 2001)
16. A.A. Kittur, M.Y. Kariduraganavar, U.S. Toti, K. Ramesh, T.M. Aminabhavi, J. Appl. Polym. Sci. **90**, 2441–2448 (2003)
17. H. van Heyden, S. Mintova, T. Bein, Chem. Mater. **20**, 2956–2963 (2008)
18. M. Dai, J. Colloid Interface Sci. **164**, 223–228 (1994)
19. Ş. Sert, C. Kütahyali, S. İnan, Z. Talip, B. Çetinkaya, M. Eral, Hydrometallurgy **90**, 13–18 (2008)
20. X. Han, W. Wang, X. Ma, Chem. Eng. J. **171**, 1–8 (2011)
21. J. Zhang, D. Cai, G. Zhang, C. Cai, C. Zhang, G. Qiu, K. Zheng, Z. Wu, Appl. Clay Sci. **83–84**, 137–143 (2013)
22. Y. Liu, Y. Kang, B. Mu, A. Wang, Chem. Eng. J. **237**, 403–410 (2014)
23. Y. Bulut, H. Aydın, Desalination **194**, 259–267 (2006)
24. Y.S. Ho, G. McKay, Process Biochem. **34**, 451–465 (1999)
25. D. Pathania, S. Sharma, P. Singh, Arab. J. Chem. (2013). doi:10.1016/j.arabjc.2013.04.021
26. Y. Li, Q. Du, T. Liu, J. Sun, Y. Wang, S. Wu, Z. Wang, Y. Xia, L. Xia, Carbohydr. Polym. **95**, 501–507 (2013)
27. C.-H. Wang, B.J. Hwang, Chem. Eng. Sci. **55**, 4311–4321 (2000)
28. M. Ghaedi, M.D. Ghazanfarkhani, S. Khodadoust, N. Sohrabi, M. Oftade, J. Ind. Eng. Chem. **20**, 2548–2560 (2014)
29. Z. Kong, X. Li, J. Tian, J. Yang, S. Sun, J. Environ. Manag. **134**, 109–116 (2014)